A novel approach to digital beamforming

Roger G. Pridham and Ronald A. Mucci

Raytheon Company, Submarine Signal Division, Portsmouth, Rhode Island 02871
(Received 13 June 1977; revised 29 September 1977)

For many sonar applications, the sensor outputs of a hydrophone array are sampled at a rate significantly higher than that required for waveform reconstruction when digital beamforming is used. The reason for this is that the number of synchronous, or "natural," beampointing directions is proportional to the beamformer input rate. This paper presents an implementation of a digital beamformer that achieves the desired synchronous beams while minimizing the sensor channel sampling rate requirement. The technique employs zero padding of sensor data followed by digital interpolation filters to achieve vernier beamformer delays. Interpolation filtering can be done either at the beamformer input or output to minimize processing requirements. The resulting structure realizes a hardware savings since both A/D converter and cable bandwith requirements can be traded off against digital processing complexity to achieve an optimal partitioning.

PACS numbers: 43.60.Gk, 43.30.Vh

INTRODUCTION

A beamformer can be interpreted as a spatial filter which operates on the outputs of an array of sensors in order to enhance the amplitude of a coherent wavefront, which is propagating in a medium such as the ocean, relative to that of background noise and directional interferences. Conventional time-domain beamforming is accomplished by appropriately delaying and adding the shaded outputs of an array of hydrophones as indicated in Fig. 1. The shading or weighting of the sensor outputs is done to improve the beam's spatial response. Typically, the beam delays are matched to the anticipated propagation delays of a pressure field incident from a specific direction. The beamformer function can be implemented either in analog or digital hardware.

A digital implementation requires that the output of each hydrophone be sampled in time prior to beamforming as shown in Fig. 2. These sets of discrete data samples are then time delayed and summed in the beamforming operation. It is well known that a signal must be sampled at a rate consistent with Nyquist criterion[1] in order to permit reconstruction of the waveform. In particular, it is desirable that samples of the beam *output* be computed at this rate. For a low-pass signal, this minimum sampling rate is twice the highest frequency of the signal spectrum.

However, also to be considered in regard to the sampling rate at the beam *input* are the requirements on the quantization of the time delays $\tau_n(n = 1, \ldots)$. These delays are quantized to increments of the input sampling interval. For a given quantization there is a discrete set of "look directions" which can be achieved exactly. These exact beams are referred to as synchronous, or "natural," beams. The number of synchronous beampointing directions increases with the input sampling rate.

For many applications, digital beamformers require an input rate which is significantly higher than that required for waveform reconstruction in order to achieve an adequate set of synchronous beampointing directions.[2] In some cases, this high sampling rate requires a prohibitive number of A/D converters. Also, the high sampling rate may impose stringent requirements on the bandwidth of the cables which connect the A/D converters and beamformer. This latter problem can be particularly significant if there is a large physical distance between the A/D converters and the digital processor.

An obvious alternative is to form nonsynchronous beams using the coarsely quantized time-delay set available at the low sampling rate needed to reconstruct the waveform. Usually, this alternative is rejected because of the relatively poor beam patterns of these "approximate" beams.[2] In fact, the quality of the nonsynchronous beams can be improved only by increasing the input rate.

This paper presents another approach which requires samples at a rate consistent with the Nyquist criterion. The desired time-delay quantization associated with the high sample rate is achieved by digital interpolation of the sampled data. Hence, additional digital computation capability is required to perform the interpolation function. However, as discussed here, the interpolation can be performed efficiently using Finite Impulse Response (FIR) digital filters.

This principle is a simple one, but its consequences are extremely significant; that is, the hardware impact of the high data rate on A/D converter and cable bandwidth can now be shared with the digital processor in order to optimize system implementation.

An even more interesting aspect of this approach concerns the relationship between beamforming and interpolation. Digital interpolation can be viewed as a two-step process[3,4] where the data sequence is first zero padded and then processed with a linear, digital interpolation filter. Since the beamformer operation is linear, the interpolation filtering can be done either at the beamformer input or output as illustrated in Fig. 3.

When the interpolation is done at the beamformer input [Fig. 3(a)], the operation of the beamformer is equivalent to the conventional approach shown in Fig. 2,

 0001-4966/78/6302-0425$00.80

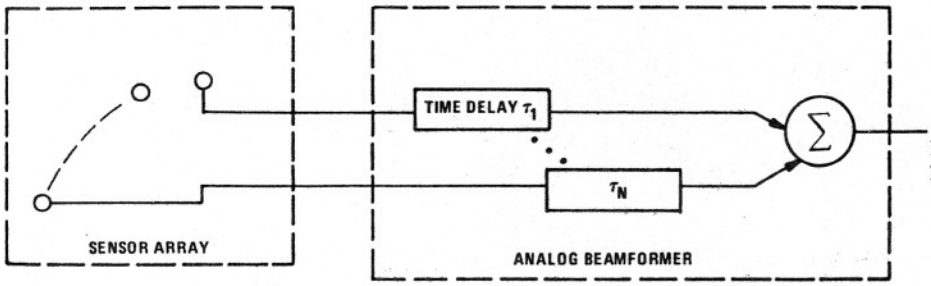

FIG. 1. Beamformer and antenna array of hydrophone elements.

where the output sample rate is much lower than the input sample rate. However, when the filter is implemented at the beam output [Fig. 3(b)], the beamformer operates in a fundamentally different way: The beamformer processes the zero-padded sequences, and the input and output sample rates are identical. Down sampling to the rate required for waveform reconstruction is achieved in the interpolation filter.

In subsequent discussion, it will be shown that this latter implementation is more computationally efficient if the number of simultaneously formed beams is less than the number of elements. In addition, interpolation at the beam output permits a substantial reduction in the memory required for delay sum beamforming.

In the following sections, the concept of digital interpolation beamforming is presented. Expressions are also derived for the error introduced by the interpolation operation. The results indicate that this error is controllable and quite small for an interpolation filter of "modest" design.

I. BEAMFORMER DESCRIPTION

Beamforming is realized by delaying and summing the shaded outputs of the array of sensors. If the beam output is denoted $b(t)$, then

$$b(t) = \sum_{n=1}^{N_E} x_n(t - \tau_n), \tag{1}$$

where τ_n is the time delay required to compensate for the delay experienced by a coherent wavefront propagating from a specified direction to the nth sensor of an array of N_E sensors, and $x_n(\cdot)$ denotes the shaded output voltage of the nth sensor. (The shading weights, without loss of generality, are suppressed to simplify notation.) The specified direction to which the time delays (τ_n) phase the array is referred to as the Maximum Response Axis (MRA).

A digital implementation of (1) requires that the sensor outputs be sampled and, thus, that the time delays be quantized to the accuracy of the sampling interval. Let δ denote the fine sampling interval needed to achieve the delay quantization requirement. The sampling interval needed to satisfy the Nyquist criterion is Δ, where, as mentioned previously,

$$\Delta > \delta. \tag{2a}$$

Corresponding to δ and Δ are the sampling frequencies $f_\delta = \delta^{-1}$ and $f_\Delta = \Delta^{-1}$, where

$$f_\Delta < f_\delta. \tag{2b}$$

In subsequent analysis it is assumed that δ is an integer multiple of Δ. Specifically,

$$\Delta = L\delta, \tag{3}$$

where L is an integer such that $L > 1$. Also, time delays are quantized to an integer multiple of δ, i.e.,

$$\tau_n = M_n\delta, \tag{4}$$

where M_n is the rounded integer part of the quotient $\tau_n\delta^{-1}$.

The beamformer output samples can be computed at an interval $K\delta$, where K is an integer not equal to L. However, in order to simplify the discussion, it is assumed that the digital beamformer computes $b(m\Delta)$, where

$$b(m\Delta) = \sum_{n=1}^{N_E} x_n[(mL - M_n)\delta]. \tag{5}$$

Extension to the general beamformer down-sampling case, where the beam output interval is $L^{-1}K\Delta$, is readily made for all the results given in this paper.

A graphical interpretation of (5) is given in Fig. 4. A/D converters provide samples of the continuous wavefronts at the interval δ. The digital beamformer introduces the delays necessary to sum the data samples along the indicated lines. Output values $b(m\Delta)$ are computed at the rate f_Δ needed to reconstruct the beam output.

For the conventional approach, the total sampling

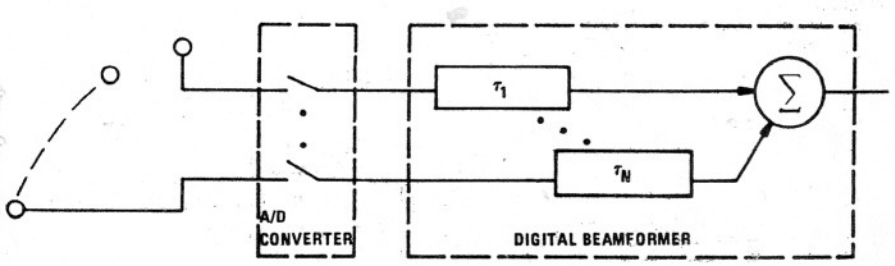

FIG. 2. Digital beamforming operation.

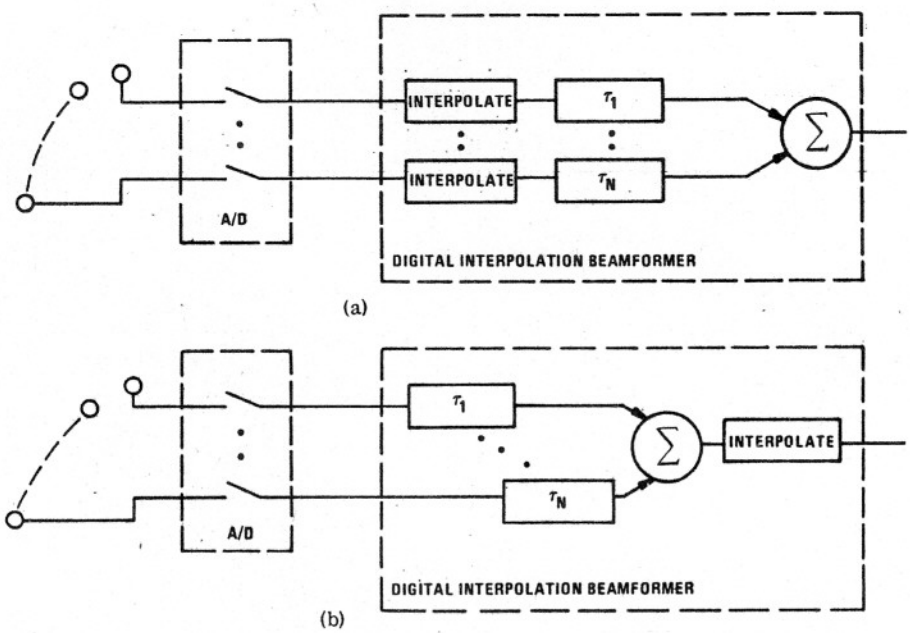

FIG. 3. Two implementations for interpolation beamforming: (a) interpolation filter before beamformer, and (b) interpolation filter after beamformer.

requirements are $N_E f_\delta$ samples/s. Digital beamformer computation requires $N_B(N_E - 1)f_\Delta$ real additions/s, where N_B is the number of beams.

For the interpolation technique, the N_E sensors are sampled at the interval Δ. The vernier sampling interval δ is realized by interpolating these samples using the procedure outlined in Appendix A. In this case, the beamformer output is

$$\hat{b}(m\Delta) = \sum_{n=1}^{N_E} \hat{x}_n[(mL - M_n)\delta], \tag{6}$$

where the symbol ($\hat{}$) is used to denote the interpolation approximation. Interpolation is achieved in two steps.[3,4] First, $L - 1$ zeros are padded between each sample to form the sequence $v(m\delta)$, where

$$v_n(m\delta) = \begin{cases} x_n(mL^{-1}\Delta), & \text{for } m = 0, \pm L, \pm 2L, \ldots \\ 0, & \text{otherwise.} \end{cases} \tag{7}$$

This padded sequence is filtered with an interpolation filter, identical for each hydrophone, to obtain $\hat{x}_n(m\delta)$, which approximates $x_n(m\delta)$. The accuracy of the approximation is determined by the interpolation filter. Figure 5 illustrates this interpretation of the digital interpolation process, an interpretation which is particularly useful for describing the new beamforming technique.

Figure 6 shows how the beamformer operates on the interpolated sequences. The timing is identical with that shown in Fig. 4. The difference is that the beamformer operates on data obtained from the interpolation filter rather than that directly obtained from the A/D converter. This difference permits greater multiplexing of A/D converters. The price paid for the increased A/D converter multiplexing capability is that additional operations are required to implement the interpolation filters. However, the computation is simplified since most of the input values are zeros.

Interpolation beamforming requires a total A/D rate of only $N_E f_\Delta$ samples/s. Thus, the bandwidth requirements are reduced by a factor of L, representing a possible significant reduction in complexity and cost. As before, the beamforming operation requires $N_B(N_E - 1)f_\Delta$ real additions/s. However, in order to implement the interpolation filters, $N_E(N_C/L)f_\delta$ real multiplies/s, and $N_E(N_C/L - 1)f_\delta$ real additions/s are required, where N_C is the number of filter coefficients. The tradeoff is between reduction of bandwidth and A/D requirements, and digital processor requirements.

An alternate implementation of the approach, which has an advantage if there are more hydrophones than

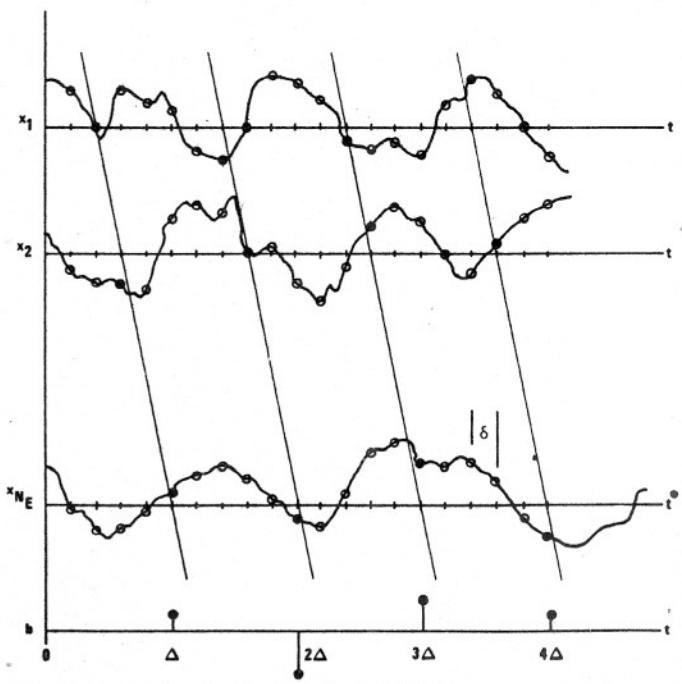

FIG. 4. Input/output timing relationship for conventional time-domain digital beamformer.

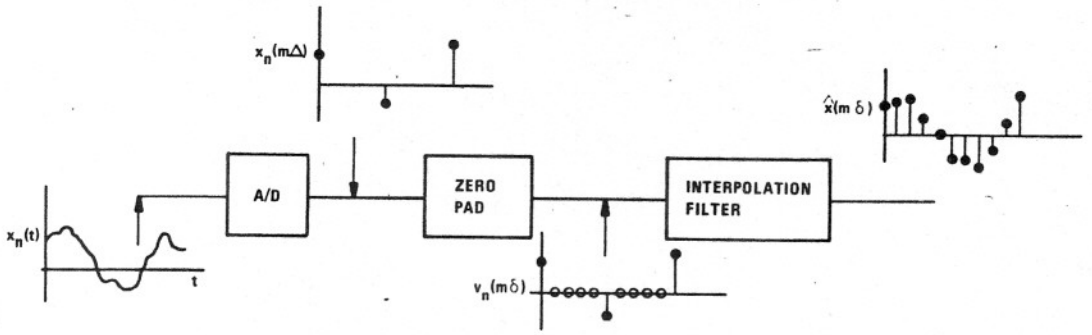

FIG. 5. Two-step interpolation process.

ber , obtained by interchanging the beamformer and the interpolation filter, is shown in Fig. 7. The two implementations are equivalent if all of the interpolation filters are identical since filtering and beamforming are linear operations that can be interchanged. For this approach, the beamformer operates on the sequence $v_n(m\delta)$ to obtain an output sequence $\hat{b}(m\delta)$ at the time interval δ. Downsampling occurs in the interpolation filter rather than in the beamformer. The interpolation filter smooths this sequence to obtain an accurate representation of the beamformer output $\hat{b}(m\Delta)$ at the time interval Δ. As for the previous implementation, the sensor sampling requirement is $N_E f_\Delta$ samples/s. However, since interpolation is done at the beam output, $N_B N_C f_\Delta$ multiplies/s and $N_B(N_C-1)f_\Delta$ additions/s are required.

Although the beam output must be computed at the high rate f_δ, the input to the beamformer consists primarily of zeros. Beamformers exist which are microprogrammable,[5] and they can be programmed to take advantage of the periodically recurring zeros. Hence, the higher beam computation rate does not necessarily impact on the computational requirements of the beamformer. Clearly, since $f_\delta = L f_\Delta$, the placing of the filter at the beamformer input (output) has a computational advantage if there are more beams (hydrophones) than hydrophones (beams).

For delay sum beamforming it is also possible to take advantage of the padded zeros in another way in order to reduce storage memory. The sensor data need only be stored at the interval Δ. This method results in a decrease in memory size requirements by the factor L.

II. INTERPOLATION FILTER IMPLEMENTATION

As discussed in Appendix A and Sec. III, the accuracy of this procedure depends on how well the interpolation

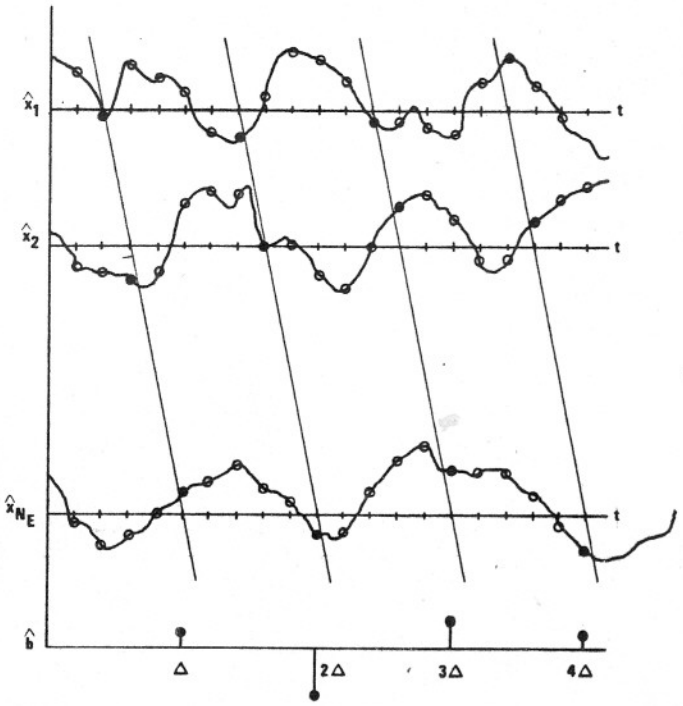

FIG. 6. Input/output timing relationship for interpolation beamforming where $\hat{x}_k(m\Delta)$ is obtained from interpolated hydrophone outputs.

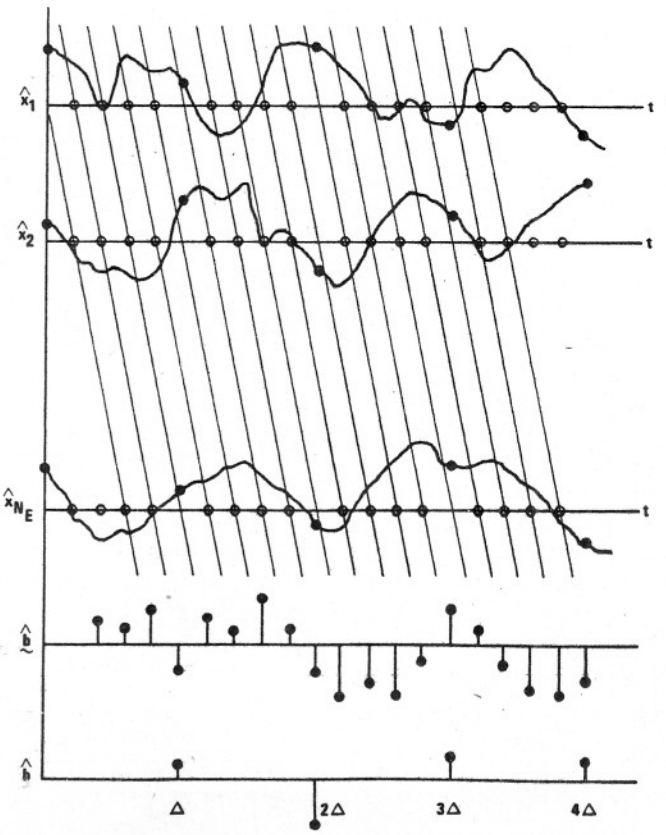

FIG. 7. Input/output timing relationship for interpolation beamforming where $\hat{b}(m\Delta)$ is obtained from interpolated beamformer outputs.

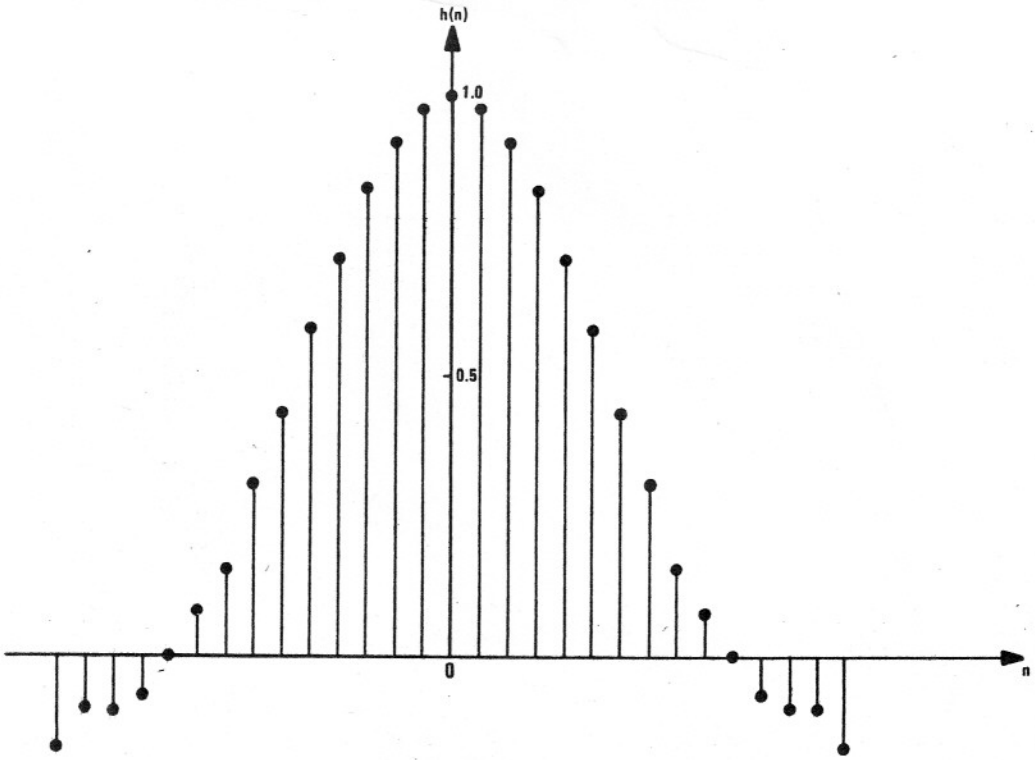

FIG. 8. Interpolation filter unit sample response for given design conditions.

filter approximates an ideal low-pass filter. In particular, the filter must attenuate undesired replica spectra associated with the zero-padding process. The goal is to minimize the passband and stopband ripple of the filter response while using a reasonably small number of filter coefficients.

Both Infinite Impulse Response (IIR) and Finite Impulse Response (FIR) digital filters can be designed which possess the desirable characteristics. However, FIR filters can be implemented nonrecursively and offer a number of advantages in this particular application. If the interpolation is performed at the hydrophone outputs, the input sequence consists primarily of zeros. Since a nonrecursive filter does not "feed back" the output data, the filter can be designed to ignore the periodically occurring zeros and to perform only the required multiplications. If the interpolation is performed at the beamformer output, the filter output need only be computed at the lower sampling rate f_Δ. Again, since there is no feedback, only those computations which are necessary to produce the desired output values are required. These advantages are lost with a recursive filter since the values fed back and combined with the input are generally nonzero. In addition, the computational and storage requirements can be minimized by implementing the overall FIR filter in stages as described in Refs. 3, 4, 6, and 7. The application of symmetric FIR filters to the interpolation process also affords the advantages of introducing a linear phase delay and, hence, no phase distortion. Also, by taking advantage of coefficient symmetry, the number of computational operations is reduced.

As an example, a symmetric FIR filter has been designed for the following values of the system design parameters:

$f_\Delta = 20$ kHz,

$f_6 = 200$ kHz,

$f_U = 5$ kHz, and

$N_C = 31$,

where f_U denotes the upper passband cutoff of interest. The filter coefficients are synthesized using the Parks and McClellan design algorithm[8] for

$$f_{U,N} = 5/200$$

and

$$f_{l,N} = 15/200,$$

where $f_{U,N}$ and $f_{l,N}$ denote the filter's upper passband edge and the lower stopband edge, respectively, normalized by f_6. Equal ripple is specified for both bands. The filter impulse response is shown in Fig. 8, and the corresponding filter frequency transfer function is given in Fig. 9.

Since L is 10, the throughput rate is 620 kHz. For symmetric FIR filters it may be possible to relax this throughput requirement by approximately a factor of 2 by taking advantage of the filter coefficient symmetry. In addition, this rate can be reduced further by designing multiple-stopband FIR filters as discussed in Refs. 4, 6, 7, and 9.

Since the FIR filter does not have the ideal low-pass filter characteristics, error is introduced at the beamformer output. This error is induced by the finite passband and stopband ripple and can be controlled by proper filter design. However, reduction of ripple generally requires an increased number of filter coefficients. Thus, a tradeoff between accuracy and computational complexity arises.

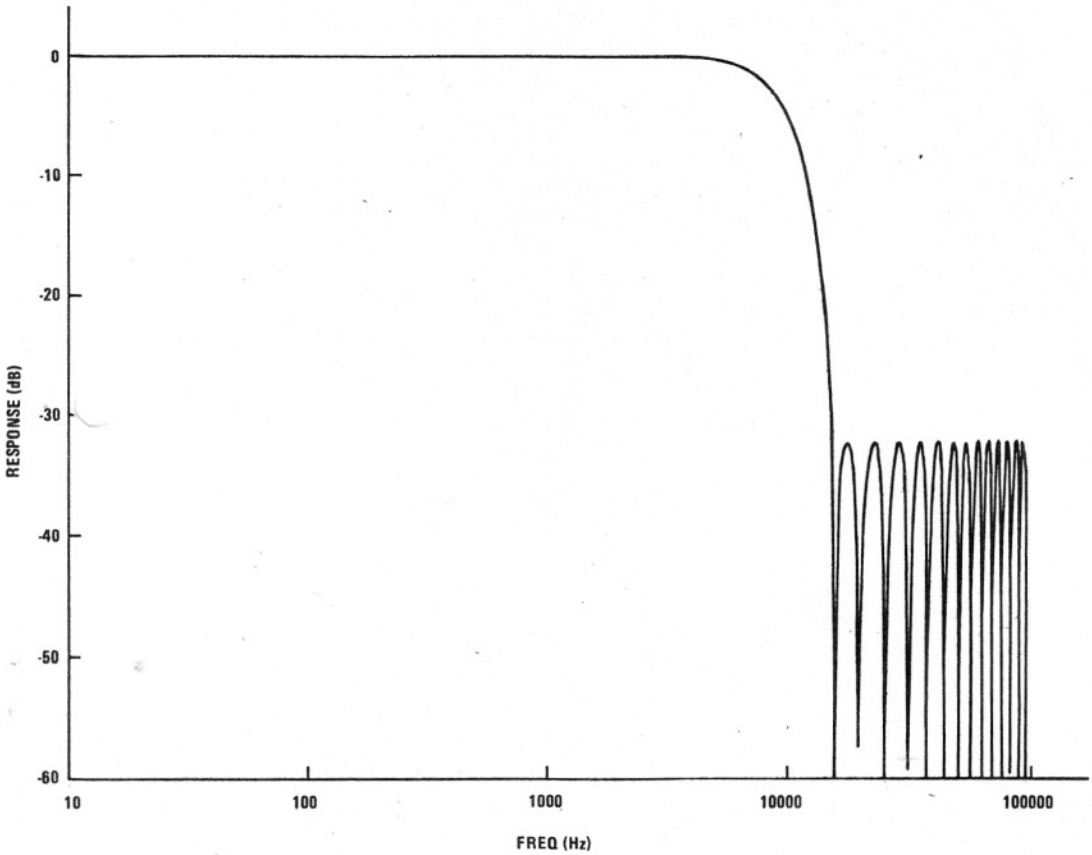

FIG. 9. Frequency characteristics for 31-coefficient interpolation filter.

III. ANALYSIS

In this section, expressions are derived for the Fourier transform of digital beamformer output sequences. First, a conventional time-domain digital beamformer structure is discussed. Then, a structure using the new interpolation technique is considered. These results show how the interpolation error can be interpreted in terms of the passband and stopband ripple of the interpolation filter acting at the beamformer output. The expressions derived in this section make use of fundamental results obtained in Appendix A. It may be advisable for the reader to review Appendix A before continuing with this section. It should be noted that lower-case symbols represent sample sequences while upper-case notation is used for the corresponding Fourier transforms.

A. Conventional digital beamformer

The Fourier transform of $b(m\Delta)$ given by Eqs. (5) and (A2) is

$$B[\exp(i\omega\Delta)] = \sum_{m=-\infty}^{\infty} b(m\Delta)\exp(-im\,\omega\Delta)$$

$$= \sum_{n=1}^{N_E}\left\{\sum_{m=-\infty}^{\infty} x_n[(mL - M_n)\delta]\exp(-im\omega\Delta)\right\}. \tag{8}$$

The results of Appendix A can be used to evaluate the sum on m. Specifically, from Eqs. (A9) and (A14),

$$B[\exp(i\omega\Delta)] = L^{-1}\sum_{k=0}^{L-1}\sum_{n=1}^{N_E}\exp[-i(\omega\Delta - 2\pi k)M_n L^{-1}]$$

$$\times X_n\{\exp[i(\omega\Delta - 2\pi k)L^{-1}]\}, \tag{9}$$

where $X_n(\cdot)$ is the Fourier transform of the sequence $x_n(m\delta)$, i.e.,

$$X_n[\exp(i\omega\delta)] = \sum_{m=-\infty}^{\infty} x_n(m\delta)\exp(-im\omega\delta). \tag{10}$$

If the sampling interval Δ is adequate for reconstruction of the sensor outputs, then the overlap of the $k=0$ spectrum and the $k\neq 0$ spectra is negligible. In this case, for the frequency range of interest (i.e., $0 \leq \omega \leq 2\pi\Delta^{-1}$), one has

$$B[\exp(i\omega\Delta)] = L^{-1}\sum_{n=1}^{N_E}\exp(-i\omega\Delta M_n L^{-1})X_n[\exp(i\omega\Delta L^{-1})]. \tag{11}$$

This approximation is exact if the $x_n(t)$ are precisely bandlimited.

B. Interpolation digital beamformer

For interpolation beamforming, the beamformer output is $\hat{b}(m\Delta)$ as given by (6). The Fourier transform of $\hat{b}(m\Delta)$ follows from Eqs. (A9) and (A14), i.e.,

$$\hat{B}[\exp(i\omega\Delta)] = L^{-1}\sum_{k=0}^{L-1}\sum_{n=1}^{N_E}\exp[-i(\omega\Delta - 2\pi k)M_n L^{-1}]$$

$$\times \hat{X}_n\{\exp[i(\omega\Delta - 2\pi k)L^{-1}]\}, \tag{12}$$

FIG. 10. Linear array of 21 equispaced omnidirectional elements.

where $\hat{B}[\exp(i\omega\Delta)]$ and $\hat{X}_n[\exp(i\omega\Delta)]$ are the Fourier transforms of $\hat{b}(m\Delta)$ and $\hat{x}(m\delta)$, respectively. Equation (A6) shows that $X_n[\exp(i\omega\delta)]$ can be expressed as

$$\hat{X}_n[\exp(i\omega\delta)] = H[\exp(i\omega\delta)]V[\exp(i\omega\delta)], \tag{13}$$

where $H[\exp(i\omega\delta)]$ is the transform of the interpolation filter unit sample response $h(m\delta)$, and $V_n[\exp(i\omega\delta)]$ is the transform of the zero-padded sequence $v_n(m\delta)$ as defined by (7). It can readily be shown that

$$V_n[\exp(i\omega\delta)] = X_n[\exp(i\omega\delta L)]. \tag{14}$$

Substitution of (13) into (12) yields

$$\hat{B}[\exp(i\omega\Delta)] = L^{-1}\sum_{k=0}^{L-1}\sum_{n=1}^{N_E}\exp[-i(\omega\Delta - 2\pi k)M_n L^{-1}] \times H\{\exp[i(\omega\Delta - 2\pi k)L^{-1}]\}V_n\{\exp[i(\omega\Delta - 2\pi k)L^{-1}]\}. \tag{15}$$

The structure suggested here consists of processing the zero-padded sequences $v_n(m\delta)$ with the interpolation filter and then computing the beam output at the rate Δ^{-1}.

A second structure is suggested by noting that the filter transform in (15) can be removed from the sum on n, i.e.,

$$\hat{B}[\exp(i\omega\Delta)] = L^{-1}\sum_{k=0}^{L-1} H\{\exp[i(\omega\Delta - 2\pi k)L^{-1}]\} \times \sum_{n=1}^{N_E}\exp[-i(\omega\Delta - 2\pi k)M_n L^{-1}]V_n\{\exp[i(\omega\Delta - 2\pi k)L^{-1}]\}. \tag{16}$$

This corresponds to performing the beamforming operation on the zero-padded sequence at the high rate f_δ, and interpolating the beam output sequence.

In order to examine these results further, (14) is substituted into (15), yielding

$$\hat{B}[\exp(i\omega\Delta)] = L^{-1}\sum_{k=0}^{L-1}\sum_{n=1}^{N_E}\exp[-i(\omega\Delta - 2\pi k)M_n L^{-1}] \times H\{\exp[i(\omega\Delta - 2\pi k)L^{-1}]\}X_n[\exp(i\omega\Delta)]. \tag{17}$$

The last step follows since

$$X_n\{\exp[i(\omega\Delta - 2\pi k)]\} = X_n[\exp(i\omega\Delta)].$$

Equation (17) can be expanded as

$$\hat{B}[\exp(i\omega\Delta)] = L^{-1}\sum_{n=1}^{N_E}\exp(-i\omega\Delta M_n L^{-1})H[\exp(i\omega\Delta L^{-1})] \times X_n[\exp(i\omega\Delta)] + L^{-1}\sum_{k=1}^{L-1}\sum_{n=1}^{N_E}X_n[\exp(i\omega\Delta)] \times\exp[-i(\omega\Delta - 2\pi k)M_n L^{-1}]H\{\exp[i(\omega\Delta - 2\pi k)L^{-1}]\}. \tag{18}$$

The $k \neq 0$ terms overlap the $k = 1$ term in the desired frequency range ($0 \le \omega \le 2\pi\,\Delta^{-1}$), unless $H[\exp(i\omega\delta)]$ is precisely limited to that band. This is true even if the $x_n(t)$ are precisely bandlimited in the desired range. Out-of-band aliasing occurs, in general, for the interpolation beamformer since the FIR interpolation filters have nonzero stopband ripple. However, as discussed in the previous section, this ripple can be made quite small if a reasonable number of coefficients are used.

The effects of the interpolation errors on the beampattern can be investigated using (18). For example, a single-frequency beam pattern was computed for the set of 31 symmetric coefficients described in the previous section. These coefficients produced an upper passband cutoff frequency of 5000 Hz for a sampling rate of 200 kHz. A line array of 21 omnidirectional elements shown in Fig. 10 was considered. The beam pattern was computed for a conventional beamformer with inputs sampled at 200 kHz for the first "synchronous" steered direction off broadside. This direction corresponds to the value of θ for which

$$(d/c)\sin\theta = f_\delta^{-1}, \tag{19}$$

where d denotes the interelement spacing, c denotes the propagation speed, and θ is the angle measured from broadside. For a half-wavelength spacing at the cutoff frequency f_U, where $f_U = 5000$,

$$\sin\theta = \frac{2c}{\lambda f_\delta} = \frac{2f_U}{f_\delta} = \frac{1}{20}. \tag{20}$$

Hence, $\theta = 2.8°$, and the corresponding beam pattern is shown in Fig. 11 as the solid line.

The beam pattern which would result from interpolation with 31 coefficients was computed using (18) for an interpolation ratio of 10:1. This is shown as the dashed line in Fig. 11. A comparison of the two beam patterns shows that the aliasing associated with the interpolation has negligible effect on the mainlobe and no significant effect on the sidelobe structure. Beampatterns were computed for other steered directions ranging from broadside to endfire for both conventional and interpolation beamforming. In all cases there was no practical degradation of beam-pattern structure.

The beam pattern was also computed using the nonsynchronous delays which result from a sampling frequency of 20 kHz. This beam pattern is also shown in Fig. 11 for comparison. It should be noted that there is appreciable degradation in both mainlobe and sidelobe structure. The apparent increase in sidelobe level results from the partially incoherent addition of the sensor outputs for a source on the beam's MRA.

IV. SUMMARY AND CONCLUSIONS

A technique for digital beamforming has been presented which relaxes the A/D conversion rate and, correspondingly, the data transmission bandwidth requirements. These hardware savings are offset by the additional hardware required for digital interpolation. However, the extra digital processing can be minimized through the use of the appropriate canonical interpolation beamformer structure and computationally efficient implementations of FIR filters. Storage memory can

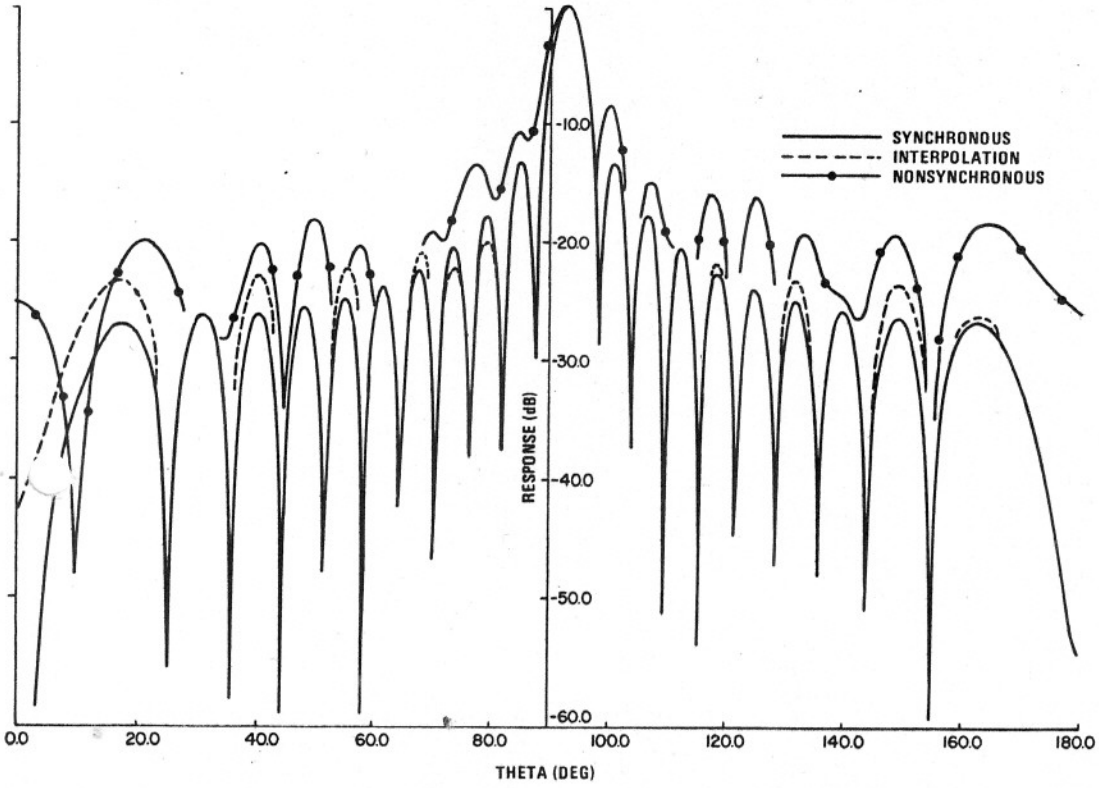

FIG. 11. Comparison for various beamformer techniques (90° corresponds to broadside).

also be reduced for delay sum beamforming from that required by a conventional time-domain digital beamformer. The degradation introduced by interpolation has been analyzed and has been shown to be small, for reasonable length filters, in comparison to that incurred for nonsynchronous beams formed with the same sensor sampling rate.

This beamformer implementation, incorporating an interpolation filter, offers a potential hardware savings since both A/D converter and cable bandwidth requirements can be traded off against digital processing complexity. However, such system parameters as number of array elements, system bandwidth, number of beams formed simultaneously, cable bandwidth requirements, digital memory, reliability and maintainability, etc., must be considered in order to achieve an optimal partitioning of hardware cost.

ACKNOWLEDGMENTS

The authors wish to express their appreciation to A. C. Callahan for helpful discussions on this topic, and also to G. F. Siletchnik for developing the computer program used for beam-pattern prediction.

APPENDIX A

This appendix gives definitions and results which are used to derive the beamformer output spectrum in Sec. III. The notation is consistent with that given in Ref. 3. Sampled sequences are denoted by lower-case letters. Z transforms are denoted using the upper case.

First, the Z transform of a sequence $x(n\Delta)$, $n = 0, \pm 1, \ldots$, is defined as

$$X(Z) = \sum_{n=-\infty}^{\infty} x(n\Delta) Z^{-n}. \tag{A1}$$

The Fourier transform of $x(n\Delta)$ is obtained by evaluating $X(Z)$ on the unit circle, i.e.,

$$X[\exp(i\omega\Delta)] = \sum_{n=-\infty}^{\infty} x(n\Delta) \exp(-in\omega\Delta). \tag{A2}$$

A sequence $v(n\delta)$ is now considered, where $\delta = L^{-1}\Delta$, with L being an integer greater than 1 [which is obtained by zero padding $x(n\Delta)$]. That is,

$$v(n\delta) = \begin{cases} x(nL^{-1}\Delta), & \text{for } n = 0, \pm L, \pm 2L, \ldots \\ 0, & \text{otherwise}. \end{cases} \tag{A3}$$

This sequence has the Fourier transform

$$V[\exp(i\omega\delta)] = \sum_{n=-\infty}^{\infty} v(n\delta) \exp(-in\omega\delta) = X[\exp(i\omega\Delta)]. \tag{A4}$$

Figure A-1 (a), (b), and (c) illustrates the relationship of the transforms $X[\exp(i\omega\Delta)]$, $V[\exp(i\omega\delta)]$, and $X[\exp(i\omega\delta)]$ for $L = 2$. It should be noted that $V[\exp(i\omega\delta)]$ is identical to $X[\exp(i\omega\delta)]$, except for the presence of replica spectra at $\omega = \pm 2\pi/\delta,\ 6\pi/\delta, \ldots$. The sequence $v(n\delta)$ can be transformed by a filtering operation into a sequence which approximates $x(n\delta)$. Specifically,

$$\hat{x}(n\delta) = \sum_{m=-\infty}^{\infty} h(m\delta) v[(n-m)\delta], \tag{A5}$$

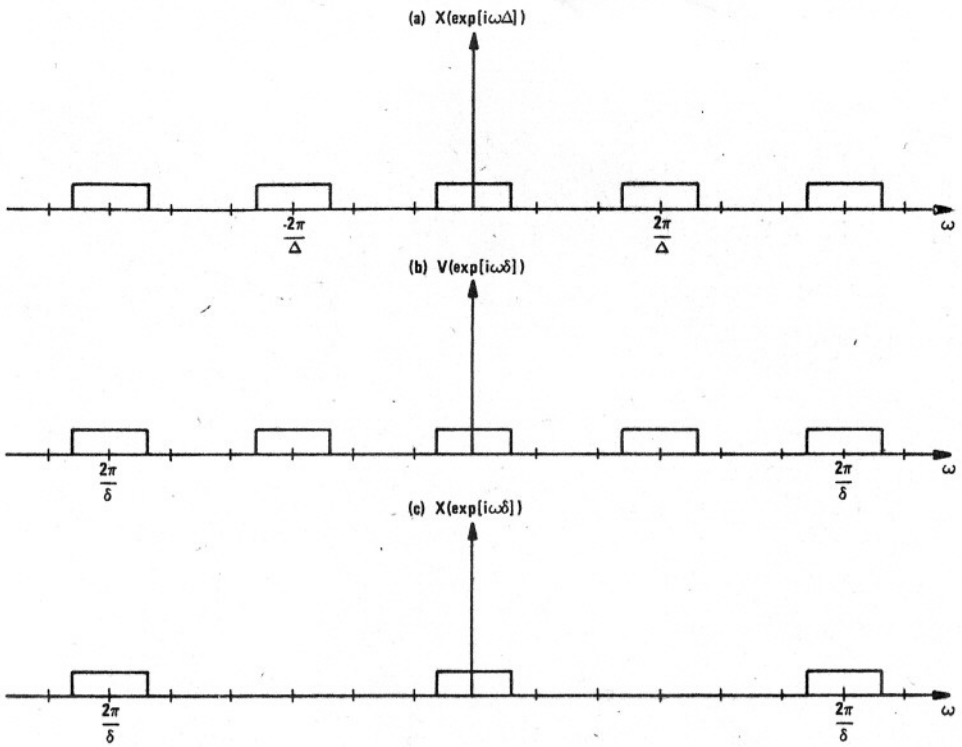

FIG. A-1. Example of Fourier transforms for the sequences (a) $x(n\Delta)$, (b) $v(n\delta)$, and (c) $x(n\delta)$ for the case $L=2$ (i.e., $\Delta=2\delta$).

where $h(m\delta)$ is the filter's unit sample response. The transform of $\hat{x}(n\delta)$ is

$$\hat{X}[\exp(i\omega\delta)] = \sum_{n=-\infty}^{\infty} \hat{x}(n\delta)Z^{-n}$$

$$= H[\exp(i\omega\delta)]V[\exp(i\omega\delta)]$$

$$= H[\exp(i\omega\delta)]X[\exp(i\omega\Delta)], \qquad \text{(A6)}$$

where $H[\exp(i\omega\delta)]$ is the Fourier transform of $h(m\delta)$.

The desired result is obtained when $H[\exp(i\omega\delta)]$ is chosen as an approximation to an ideal low-pass filter which passes the desired spectra but suppresses the undesired spectra. Figure A-2 illustrates this procedure for the example given in Fig. A-1. It should be observed that $X[\exp(i\omega\delta)]$ and $\hat{X}[\exp(i\omega\delta)]$ are identical except for perturbations due to ripple in the passband and stopband of $H[\exp(i\omega\delta)]$.

The filter design procedure given in Sec. II imple-

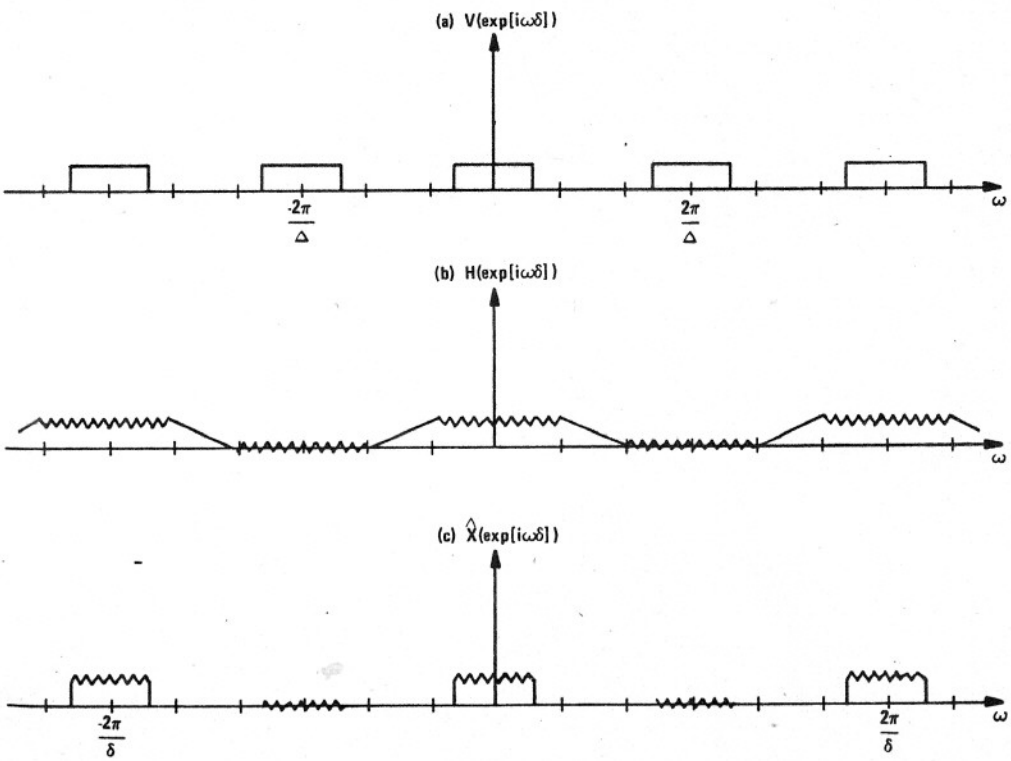

FIG. A-2. Example of filtering operation where $\hat{X}[\exp(i\omega\delta)]$ approximates $X[\exp(i\omega\delta)]$. (a) $V[\exp(i\omega\delta)]$, (b) $H[\exp(i\omega\delta)]$, and (c) $\hat{X}[\exp(i\omega\delta)]$.

ments $H[\exp(i\omega\delta)]$ with a symmetric, FIR filter. For this type of filter, one has

$$\hat{x}(n\delta) = \sum_{m=-M}^{M} h(m\delta)v[(n-m)\delta]$$

$$= \sum_{m=0}^{M} h(m\delta)\{v[(n-m)\delta] + v[(n+m)\delta]\} - h(0)v(n\delta)\,. \tag{A7}$$

Since $h(m\delta)$ is symmetric, $H[\exp(i\omega\delta)]$ is constrained to have linear phase.

The final result to be derived concerns the effect of shifting and down sampling a sequence $w(n\delta)$. Consider the sequence

$$y(n\Delta) = w[(nL-p)\delta] \tag{A8}$$

which has the Fourier transform

$$-Y[\exp(i\omega\Delta)] = \sum_{n=-\infty}^{\infty} y(n\Delta)\exp(-in\omega\Delta)$$

$$= \sum_{n=-\infty}^{\infty} w[(nL-p)\delta]\exp(-in\omega\Delta)\,. \tag{A9}$$

This expression can be written as

$$Y[\exp(i\omega\Delta)] = \sum_{n=0,\pm L,\pm 2L,\cdots} w[(n-p)\delta]\exp(-inL^{-1}\omega\Delta)$$

$$= \sum_{n=-\infty}^{\infty} w[(n-p)\delta]\,S_n\exp(-inL^{-1}\omega\Delta)\,, \tag{A10}$$

where

$$S_n = \begin{cases} 1, & n = 0, \pm L, \pm 2L, \ldots \\ 0, & \text{otherwise}\,. \end{cases} \tag{A11}$$

Since S_n has the representation

$$S_n = L^{-1}\sum_{k=0}^{L-1}\exp(i2\pi knL^{-1})\,, \tag{A12}$$

(A11) has the form

$$Y[\exp(i\omega\Delta)]$$

$$= \sum_{n=-\infty}^{\infty} w[(n-p)\delta]\left[L^{-1}\sum_{k=0}^{L-1}\exp(i2\pi knL^{-1})\right]\exp(-inL^{-1}\omega\Delta)$$

$$= L^{-1}\sum_{k=0}^{L-1}\left[\sum_{n=-\infty}^{\infty} w[(n-p)\delta]\exp[-in(\omega\delta - 2\pi kL^{-1})]\right]. \tag{A13}$$

Using the substitution $m = n-p$ yields

$$Y[\exp(i\omega\Delta)]$$

$$= L^{-1}\sum_{k=0}^{L-1}\exp[-i(\omega\Delta - 2\pi k)pL^{-1}]$$

$$\times \sum_{m=-\infty}^{\infty} w(m\delta)\exp[-i(\omega\Delta - 2\pi k)mL^{-1}]$$

$$= L^{-1}\sum_{k=0}^{L-1}\exp[-i(\omega\Delta - 2\pi k)pL^{-1}]W\{\exp[\omega\Delta - 2\pi k)L^{-1}]\}\,, \tag{A14}$$

which is the desired result.

[1] C. E. Shannon, "Communication in the Presence of Noise," Proc. IRE **37**, 10–21 (1949).

[2] G. L. DeMuth, "Frequency Domain Beamforming Techniques," IEEE Int. Conf. Acoust. Speech Signal Process. I, 713–715 (1977).

[3] R. W. Schafer and L. F. Rabiner, "A Digital Signal Processing Approach to Interpolation," Proc. IEEE **61**, 692–720 (1973).

[4] L. R. Rabiner and R. E. Crochiere, "A Novel Implementation for Narrowband FIR Digital Filters," IEEE Trans. Acoust. Speech Signal Process. ASSP-**23**, 457–464 (1975).

[5] *The Microprogrammable Beamformer* (Raytheon, Portsmouth, RI, 1974).

[6] R. E. Crochiere and L. R. Rabiner, "Optimum FIR Digital Filter Implementation for Decimation, Interpolation and Narrowband Filtering," IEEE Trans. Acoust. Speech Signal Process. **ASSP-23**, 444–456 (1975).

[7] D. W. Rorabacher, "Efficient FIR Filter Design for Sample-Rate Reduction and Interpolation," Proc. IEEE Int. Symp. Circuits Sys. **I**, 396–399 (1975).

[8] J. H. McClellan, T. W. Parks, and L. R. Rabiner, "A Computer Program for Designing Optimum FIR Linear Phase Digital Filters," IEEE Trans. Audio Electroacoust. **AU-21**, 506–526 (1973).

[9] R. E. Crochiere and L. R. Rabiner, "Further Consideration on the Design of Decimators and Interpolators," IEEE Trans. Acoust. Speech Signal Process. **ASSP-24**, 296–311 (1976).